

# Dependence of elliptic flow on number of parton degrees of freedom

Zhe Xu <sup>\*1,2</sup> and Carsten Greiner <sup>†2</sup>

<sup>1</sup>*Frankfurt Institute for Advanced Studies,*

*Ruth-Moufang-Strasse 1, D-60438 Frankfurt am Main, Germany*

<sup>2</sup>*Institut für Theoretische Physik, Goethe-Universität Frankfurt,*

*Max-von-Laue-Strasse 1, D-60438 Frankfurt am Main, Germany*

(Dated: December 3, 2018)

## Abstract

We calculate the elliptic flow parameter  $v_2$  for Au+Au collisions at  $\sqrt{s_{NN}} = 200$  GeV employing the parton cascade BAMPS (Boltzmann Approach of Multiparton Scatterings). Besides gluon interactions including the bremsstrahlung process, interactions with quarks are considered in an effective, but approximate way to investigate the dependence of the collective flow on the number of parton degrees of freedom. We find that  $v_2$  as a function of the transverse momentum  $p_T$  is sensitive to the number of parton degrees of freedom, whereas the  $p_T$  averaged  $v_2$  does not. When including quarks,  $v_2(p_T)$  shifts to lower  $p_T$ , the parton transverse momentum spectra become softer and the mean parton transverse momenta decrease.

PACS numbers: 25.75.-q, 25.75.Ld, 12.38.Mh, 24.10.Lx

---

\* xu@th.physik.uni-frankfurt.de

† carsten.greiner@th.physik.uni-frankfurt.de

## I. INTRODUCTION

Measurements on collective flow in heavy ion collisions at the BNL Relativistic Heavy Ion Collider (RHIC) [1] showed that the matter produced, the quark gluon plasma (QGP), is a nearly perfect fluid [2, 3]. Because the strength of the collective flow increases with decreasing viscosity, indirect extractions of the shear viscosity have recently been performed by tuning the shear viscosity (or the QCD coupling) as a parameter in viscous hydrodynamic [4–8] and transport models [9–11] to match the elliptic flow  $v_2$ . A consistent result has been achieved: on a conservative basis the shear viscosity to the entropy density ratio  $\eta/s$  of the QCD matter at RHIC is less than 0.4 [12]. Uncertainties stem from assumptions in modelling the various stages that the matter undergoes during its evolution.

The results from the transport calculations using the Boltzmann Approach of Multiparton Scatterings (BAMPS) [11] showed that  $v_2(p_T)$  as a function of the transverse momentum  $p_T$  is lower and the  $p_T$  spectra are harder than the experimental data, whereas the integral of both gives a  $p_T$  averaged  $v_2$ , which matches the experimental data. This inconsistency may stem from the nature of the rather complicated hadronization process than the simple parton-hadron duality picture used in [11]. Another reason may lie in the fact that only gluons are considered as interacting constituents in the calculations presented in [11]. Including quark dynamics will increase the number of parton degrees of freedom and, thus, may soften the  $p_T$  spectra and enhance  $v_2(p_T)$ . In this paper we employ BAMPS and include effective quark degrees of freedom to investigate how the increase and the equilibration of partonic multiplicities affect the elliptic flow and also the  $\eta/s$  ratio of the QGP.

This study shall demonstrate whether the buildup of elliptic flow in ultrarelativistic heavy ion collisions depends on the chemical equilibration of gluons and quarks. The latter determines the actual number of constituents in the partonic phase. In hydrodynamic calculations it is assumed that the matter stays in chemical equilibrium and thus the number of constituents is conserved. However, the situation in a real heavy ion collision might be considerably more complicated [13, 14]. Quarks are expected to achieve chemical equilibrium (if this occurs) later than gluons [13]. Even for gluons only, the chemical equilibration will proceed faster at the collision center than at the region near transverse edge of the parton system. The parton chemical equilibration can well be studied using the microscopic transport model with multiple scatterings such as BAMPS [15], because BAMPS imple-

ments perturbative QCD (pQCD) elastic collisions as well as the pQCD based inelastic bremsstrahlung incorporating full detailed balance.

The paper is organized as follows. In Sec. II we review the parton cascade BAMPS and introduce effective quarks into BAMPS as a simplification for real quark dynamics. In Sec. III the numerical results are shown to demonstrate the effect of the parton multiplicities on the elliptic flow of the parton matter. We summarize in Sec. IV.

## II. BAMPS INCLUDING EFFECTIVE QUARK DEGREES OF FREEDOM

The detailed model description of the on-shell parton cascade BAMPS can be found in Refs. [15, 16]. In short, the feature of BAMPS is the successful implementation of particle number changing processes with full detailed balance. This is ensured by using the stochastic interpretation of the transition rates in the Boltzmann equations for partons. Other parton cascade approaches can be found in [10, 17–21].

The cross section of pQCD gluon elastic scatterings is given by [11, 15]

$$\frac{d\sigma^{gg\rightarrow gg}}{d\mathbf{q}_\perp^2} = \frac{9\pi\alpha_s^2}{(\mathbf{q}_\perp^2 + m_D^2)^2} \quad (1)$$

and the effective matrix element of pQCD inspired bremsstrahlung  $gg \leftrightarrow ggg$  is taken in a Gunion-Bertsch form [13, 15, 22, 23],

$$|\mathcal{M}_{gg\rightarrow ggg}|^2 = \frac{9g^4}{2} \frac{s^2}{(\mathbf{q}_\perp^2 + m_D^2)^2} \frac{12g^2\mathbf{q}_\perp^2}{\mathbf{k}_\perp^2[(\mathbf{k}_\perp - \mathbf{q}_\perp)^2 + m_D^2]} \Theta(k_\perp \lambda_{\text{mfp}} - \cosh y), \quad (2)$$

$$|\mathcal{M}_{ggg\rightarrow gg}|^2 = |\mathcal{M}_{gg\rightarrow ggg}|^2/d_G, \quad (3)$$

where  $g^2 = 4\pi\alpha_s$  and  $d_G = 16$  is the gluon degeneracy factor for  $N_c = 3$ .  $\mathbf{q}_\perp$  denotes the perpendicular component of the momentum transfer,  $\mathbf{k}_\perp$  ( $k_\perp = |\mathbf{k}_\perp|$ ) the perpendicular component of the radiated gluon momentum and  $y$  its rapidity in the center-of-mass frame of the collision, respectively. The suppression of the bremsstrahlung due to the Landau-Pomeranchuk-Migdal effect is effectively taken into account within the Bethe-Heitler regime using the step function in Eq. (2). Gluon radiations and absorptions are only allowed if the formation time of the process, typically  $\tau = \cosh y/k_\perp$ , is shorter than the mean free path  $\lambda_{\text{mfp}}$  of the radiated or absorbed gluon.  $\lambda_{\text{mfp}}$  is calculated self-consistently [15, 24], i.m.,  $\lambda_{\text{mfp}}$  is the inverse of the total collision rate  $R_{gg\rightarrow gg} + R_{gg\rightarrow ggg} + R_{ggg\rightarrow gg}$ , where  $R_{gg\rightarrow ggg}$  and  $R_{ggg\rightarrow gg}$  also depend on  $\lambda_{\text{mfp}}$  as indicated in Eqs. (2) and (3) [see Eqs. (8), (9), (14), and (15)].

The pQCD interactions are Debye screened. The screening mass is given by [13]

$$m_D^2(\mathbf{x}, t) = \pi \alpha_s d_G \int \frac{d^3p}{(2\pi)^3} \frac{1}{p} [N_c f_g(\mathbf{x}, t, \mathbf{p}) + n_f f_q(\mathbf{x}, t, \mathbf{p})] , \quad (4)$$

where  $n_f$  is the number of quark flavor, and  $f_g$  and  $f_q$  are the distribution function of gluons and quarks at a certain quantum state. For a pure gluon matter  $f_q = 0$ .

The initial parton distribution for BAMPS calculations is the same as that chosen in Refs. [9, 11]: an ensemble of gluon minijets with transverse momenta greater than  $p_0 = 1.4$  GeV, produced via semihard nucleon-nucleon collisions within a Glauber picture. The value of  $p_0$  was chosen by matching the parton cascade result of the final transverse energy per rapidity to the experimental data [9, 11]. Quark minijets, which take about 20% of the total parton number, are neglected for present studies, in order to easily make comparisons with the previous results obtained in [11].

To take into account the quark-gluon changing process  $gg \leftrightarrow q\bar{q}$  and the elastic as well as the bremsstrahlung process involving light quarks, we effectively enlarge the gluon degeneracy factor  $d_G$ . With a larger  $d_G$  than 16, the  $ggg \rightarrow gg$  process is suppressed [see Eq. (3)] and thus more particles (i.e. quarks) will be produced. This numerical prescription indicates two assumptions: (1) Quarks are massless. (2) The elastic and the bremsstrahlung process involving quarks are identical with those of gluons according to Eqs. (1)-(3). These assumptions lead to the same kinetic equilibration of quarks and gluons, i.e.,  $f_q \sim f_g$ . The second assumption overestimates the interaction rate of a quark approximately by the color-charge factor 9/4 due to the dominance of  $gg \rightarrow gg$ ,  $qg \rightarrow qg$ ,  $gg \leftrightarrow ggg$  and  $qg \leftrightarrow qgg$  in kinetic equilibration. The real equilibration of quarks is expected to be slower than that of gluons. Moreover, the present prescription used to include quarks cannot separate quarks from gluons. The relative fraction of the quark (or gluon) number to the total parton number is not known. Quark thermalization by real quark dynamics will be investigated in the future [25]. The simplified version used here serves as a tool to study the effect on the elliptic flow when varying the number of parton degrees of freedom.

The enlarged  $d_G$  value can be obtained when considering a fully thermalized system of quarks and gluons. In this case  $f_q = f_g$  and the parton distribution function is given by  $f = d_G f_g + d_Q f_q = (d_G + d_Q) f_g$ , where  $d_Q = 24$  is the quark degeneracy factor for  $n_f = 2$ . To include effective quark degrees of freedom in BAMPS we enlarge  $d_G$  from 16 for a pure gluon system to 40 for a quark gluon system with two flavors.

Assuming  $f_q = f_g$ , which is also valid when the kinetic and chemical equilibration of quarks and gluons proceeds identically, the screening mass Eq. (4) becomes

$$m_D^2(\mathbf{x}, t) = \frac{2}{3}\pi \alpha_s N_c \int \frac{d^3p}{(2\pi)^3} \frac{1}{p} f(\mathbf{x}, t, \mathbf{p}), \quad (5)$$

which is a factor of 2/3 smaller than the value at the beginning of the expansion, because initially there are only gluons. To make a reasonable description of the early stage, we use instead of Eq. (5)

$$m_D^2(\mathbf{x}, t) = \pi \alpha_s N_c \int \frac{d^3p}{(2\pi)^3} \frac{1}{p} f(\mathbf{x}, t, \mathbf{p}) \quad (6)$$

during the entire parton evolution. Accordingly,  $m_D^2$  is overestimated by a factor of 1.5 at the late stage of the expansion, when partons thermalize. The true screening mass will be changing from Eq. (6) to Eq. (5) in time according to the true chemical equilibration of gluons and quarks, which, however, cannot be demonstrated in the present studies. More discussions will be given in the next section.

As already considered in Refs. [9, 11] for the present BAMPS calculations, the kinetic freeze-out of particles occurs when the local energy density drops below  $e_c$ , which is assumed to be the critical value for the occurrence of hadronization. In this paper we set  $e_c = 1$  GeV fm<sup>-3</sup>, which leads to a critical temperature  $T_c = 200$  MeV for a pure gluon plasma and  $T_c = 160$  MeV for a quark gluon plasma with two quark flavors [26]. After the freeze-out partons are regarded as massless pions according to a simple parton-hadron duality picture. To consider realistic chemical and kinetic freeze-out a hadronization model and the subsequent hadron cascade should be included to BAMPS, which will be done in the future. This, of course, can also have certain influence on the findings in the next section.

### III. RESULTS

With the assumptions for the quark dynamics in BAMPS we calculate the space time evolution of the quark and gluon matter produced in Au+Au collisions at  $\sqrt{s_{NN}} = 200$  GeV. The coupling is set to be a constant  $\alpha_s = 0.6$ . We evaluate the elliptic flow parameter  $v_2$  as the average of  $(p_x^2 - p_y^2)/(p_x^2 + p_y^2)$  over particles within a certain window of momentum rapidity  $y = \frac{1}{2} \ln[(E + p_z)/(E - p_z)]$ . Figure 1 shows the buildup of the elliptic flow  $v_2$  at midrapidity  $|y| < 1$  in a Au+Au collision with an impact parameter of  $b = 8.6$  fm. The solid curve gives the result of a pure gluon matter, which was already obtained from our

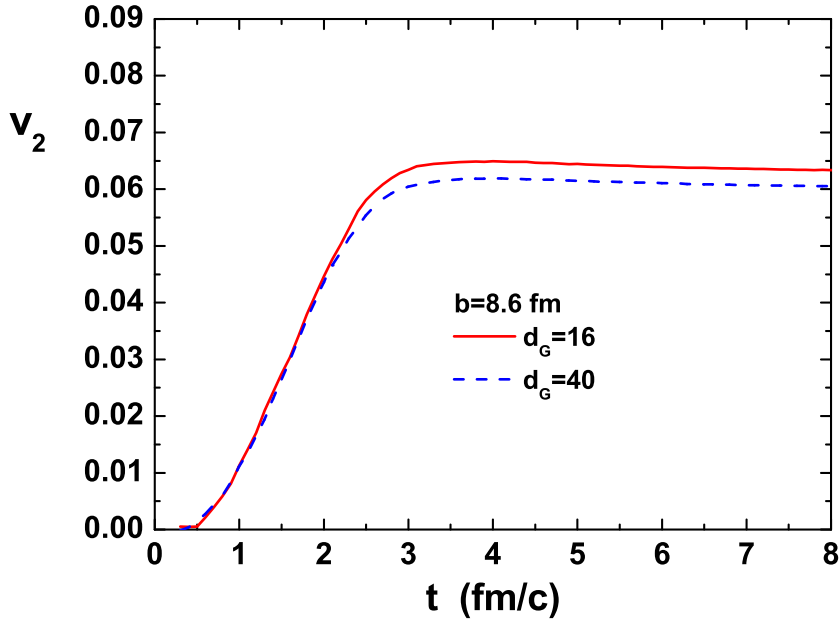


FIG. 1: (Color online) Time evolution of the  $p_T$  averaged  $v_2$  for particles within  $|y| < 1$ .

previous work [9]. The dashed curve shows the new result including quarks effectively with the enlarged  $d_G = 40$ . We see a perfect agreement between the two results except for a difference of about 5% at later times. The key quantity to understand this agreement was proposed to be the collision rate per particle  $R = n\langle\sigma\rangle$  (or similarly the Knudsen number [27]): For a fixed collision geometry and a given initial condition the  $v_2$  generation depends only on  $R$ , but not on the particular details of interactions among constituent particles. With more degrees of freedom (larger  $d_G$ ) the total particle density  $n$  becomes larger due to the production of quarks. On the other hand, the screening mass (6) also becomes larger, which decreases the total cross section  $\langle\sigma\rangle$  of all the interaction types [see Eqs. (1)-(3)]. The increase of  $n$  and the decrease of  $\langle\sigma\rangle$  could keep the collision rate per particle and thus the  $v_2$  unchanged.

To obtain a quantitative answer to this issue, we calculate numerically the total collision rate per particle  $R_{gg\rightarrow gg} + R_{gg\rightarrow ggg} + R_{ggg\rightarrow gg}$ , where

$$R_{gg\rightarrow gg} = n\langle v_{\text{rel}}\sigma_{gg\rightarrow gg}\rangle_2 \quad (7)$$

$$R_{gg\rightarrow ggg} = n\langle v_{\text{rel}}\sigma_{gg\rightarrow ggg}\rangle_2 \quad (8)$$

$$R_{ggg\rightarrow gg} = \frac{1}{2}n^2\left\langle\frac{I_{ggg\rightarrow gg}}{8E_1E_2E_3}\right\rangle_3. \quad (9)$$

The averages are defined as

$$\langle \mathcal{O} \rangle_2 = \frac{1}{n^2} \int d\Gamma_1 d\Gamma_2 f_1(x, p_1) f_2(x, p_2) \mathcal{O}, \quad (10)$$

$$\langle \mathcal{Q} \rangle_3 = \frac{1}{n^3} \int d\Gamma_1 d\Gamma_2 d\Gamma_3 f_1(x, p_1) f_2(x, p_2) f_3(x, p_3) \mathcal{Q} \quad (11)$$

with

$$n = \int d\Gamma_1 f(x, p_1), \quad (12)$$

where  $d\Gamma_j = d^3p_j/(2\pi)^3$ ,  $j = 1, 2, 3$ , and the local particle distribution function  $f(x, p)$  is the output from the parton cascade,  $f(x, p) = \sum_i \delta^{(3)}[\vec{x} - \vec{x}_i(t)] \delta^{(3)}[\vec{p} - \vec{p}_i]$ . The sum runs over all particles with individual position  $\vec{x}_i$  and momentum  $\vec{p}_i$  at time  $t$ .

For a  $gg \rightarrow gg$  or a  $gg \rightarrow ggg$  process involving two incoming particles with  $(x, p_1)$  and  $(x, p_2)$  the relative velocity of the two particles is given by  $v_{\text{rel}} = s/(2E_1E_2)$ , where  $s = (p_1 + p_2)^2$  is the invariant mass. The total cross sections read

$$\sigma_{gg \rightarrow gg} = \frac{1}{2!} \int_0^{s/4} d\mathbf{q}_\perp^2 \frac{d\sigma_{gg \rightarrow gg}}{d\mathbf{q}_\perp^2}, \quad (13)$$

$$\sigma_{gg \rightarrow ggg} = \frac{1}{2s} \int d\Gamma'_1 d\Gamma'_2 d\Gamma'_3 |\mathcal{M}_{gg \rightarrow ggg}|^2 (2\pi)^4 \delta^{(4)}(p_1 + p_2 - p'_1 - p'_2 - p'_3), \quad (14)$$

where  $d\Gamma'_j = d^3p'_j/(2\pi)^3/(2E'_j)$ ,  $j = 1, 2, 3$ . For a  $ggg \rightarrow gg$  process we define

$$I_{ggg \rightarrow gg} = \frac{1}{2!} \int d\Gamma'_1 d\Gamma'_2 |\mathcal{M}_{ggg \rightarrow gg}|^2 (2\pi)^4 \delta^{(4)}(p_1 + p_2 + p_3 - p'_1 - p'_2), \quad (15)$$

which is, similar as a cross section, an integral over the final states. The factor of  $1/2!$  in Eqs. (13) and (15) is due to the fact that the two outgoing gluons are identical particles. There is no such a factor ( $1/3!$ ) in  $gg \rightarrow ggg$  processes [28], because the three outgoing gluons are distinguished as the radiated gluon ( $p'_3$ ), the radiating gluon ( $p'_2$ ) and the gluon ( $p'_1$ ), which is only deflected and does not radiate. Thus, they are kinematically “distinguishable” particles.

We note that  $n$  in Eq. (12) is the local particle density in the center of mass frame of the Au+Au collision (collision frame) and only equals the Lorentz invariant particle density if the local particle system is at rest, e.g. at the collision center. Also the local collision rates (7)-(9) are calculated in the collision frame and are smaller than those in the rest frame by a Lorentz factor.

The left panel of Fig. 2 shows the time evolution of the total collision rate per particle  $\langle R_{gg \rightarrow gg} + R_{gg \rightarrow ggg} + R_{ggg \rightarrow gg} \rangle$ . The rate is obtained as the average over all particles in

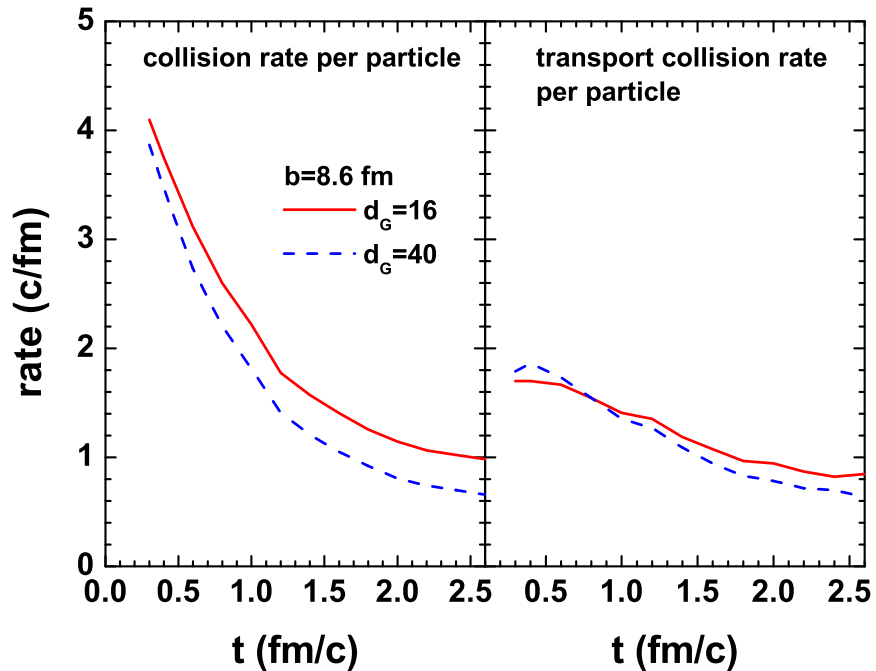


FIG. 2: (Color online) Time evolution of the collision rate (left) and the transport collision rate (right) per particle at midrapidity  $|\eta_s| < 0.2$ .

the whole transverse plan at the central space time rapidity  $|\eta_s| < 0.2$ .  $\eta_s$  is defined as  $\eta_s = \frac{1}{2} \ln[(t+z)/(t-z)]$ . The local rate per particle is calculated according to (7)-(9). We have also computed the average rate by counting interaction events, which occur in BAMPS within certain time intervals. The results from both calculations agree with each other.

As mentioned before, the collision rate per particle, may determine the buildup of the elliptic flow  $v_2$ , which is shown in Fig. 1 within the momentum rapidity  $|y| < 1$ . We have also calculated  $v_2$  within  $|\eta_s| < 0.2$ . The agreement of the two curves seen in Fig. 1 is unchanged. The reason why we show the  $v_2$  result within  $|y| < 1$  is to compare it with the experimental data (see Fig. 3).

From Fig. 2 we see a moderate difference between the collision rates in the simulations with  $d_G = 16$  and  $d_G = 40$ , whereas the average *transport* collision rates per particle shown in the right panel are much closer to each other. The slightly smaller transport collision rate in the calculation with  $d_G = 40$ , compared to that with  $d_G = 16$ , is the reason for the slightly smaller final  $v_2$  with  $d_G = 40$  than that with  $d_G = 16$  (see Fig. 1).



The local transport collision rate per particle is given by [16]

$$R_i^{\text{tr}} = \frac{\int d\Gamma_1 \frac{p_{z1}^2}{E_1^2} C_i[f] - \langle \frac{p_{z1}^2}{E_1^2} \rangle \int d\Gamma_1 C_i[f]}{n \left( \frac{1}{3} - \langle \frac{p_{z1}^2}{E_1^2} \rangle \right)}, \quad (16)$$

where  $\langle \mathcal{O} \rangle = (1/n) \int d\Gamma_1 f_1(x, p_1) \mathcal{O}$  and  $C_i[f]$ ,  $i = gg \rightarrow gg, gg \rightarrow ggg, ggg \rightarrow gg$ , denotes the respective collision term [16]. The transport collision rate per particle quantifies the time scale of thermal equilibration [16]. Because the angle  $\theta_1$  in  $p_{z1}^2/E_1^2 = \cos^2 \theta_1$  enters both the gain and loss term of  $C_i[f]$ , the larger the mean momentum deflection in each collision, the larger is the transport collision rate and the faster is the momentum isotropization. The latter leads to a faster buildup of the pressure gradient and thus to a larger elliptic flow. Therefore, the transport collision rate, rather than the collision rate, relates more closely to the buildup of the elliptic flow  $v_2$ , as demonstrated in Fig. 2 in relation with Fig. 1.

The resulting smaller difference in the total transport collision rates than that in the total collision rates (when varying  $d_G$  from 16 to 40) stems from the time evolution of the screening mass  $m_D$  [see Eq. (6)], which determines not only the cross sections  $\sigma_{gg \rightarrow gg}$ ,  $\sigma_{gg \rightarrow ggg}$ , and  $I_{ggg \rightarrow gg}$ , but also the collision angle in these processes. As mentioned after Eq. (5), the choice of  $m_D$  is physically reasonable, because the dynamics at the early stage is dominated by gluons. On the other hand,  $m_D$  is overestimated at the late times, when “quarks” have considerable fraction of the whole parton system. Thus, the cross sections and the rates at the late times shown in Fig. 2 are somewhat smaller than their true values, when the fully realistic quark dynamics is considered.

In Fig. 3 we show the final elliptic flow  $v_2$  within  $|y| < 1$  for various mean numbers of participating nucleons  $\langle N_{\text{part}} \rangle$  (equivalently impact parameters  $b$  [11]). The open squares (or the solid curves) in Fig. 3 and all the following figures depict the results from the calculations with  $d_G = 16$ , which have already been presented in Ref. [11]. The open circles show the new results with  $d_G = 40$ , which are slightly smaller than the values calculated with  $d_G = 16$  (as also seen in Fig. 1), and are still comparable with the experimental data at RHIC [29, 30].

Figure 4 presents the final transverse energies at midrapidity. If quarks are included in the initial condition for the parton cascade calculations, the results would be closer to the experimental data [31]. Comparing the results obtained in the calculations with  $d_G = 40$  to those with  $d_G = 16$ , we find a tiny difference. This implies the same decrease of the

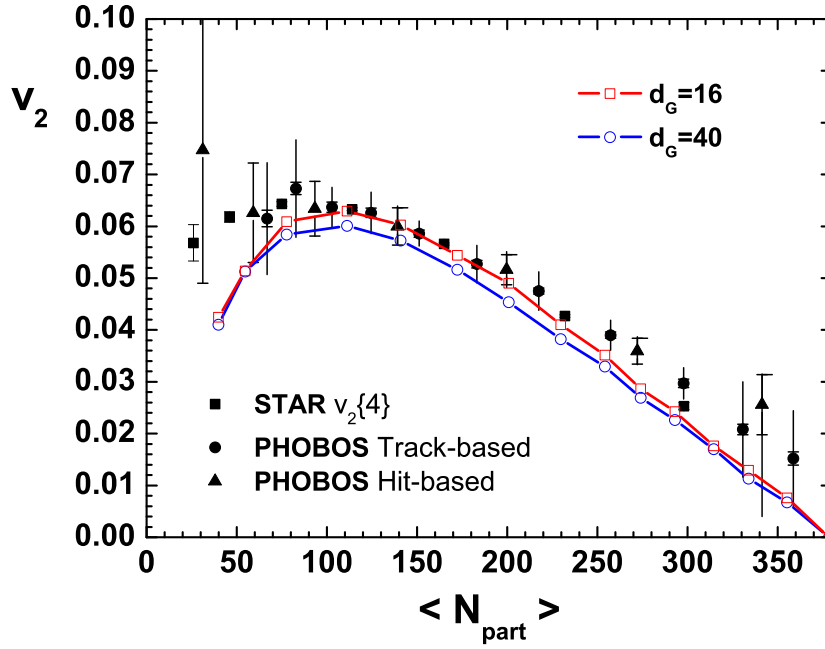


FIG. 3: (Color online) Elliptic flow parameter  $v_2$  ( $p_T$  averaged) at midrapidity as a function of number of participating nucleons.

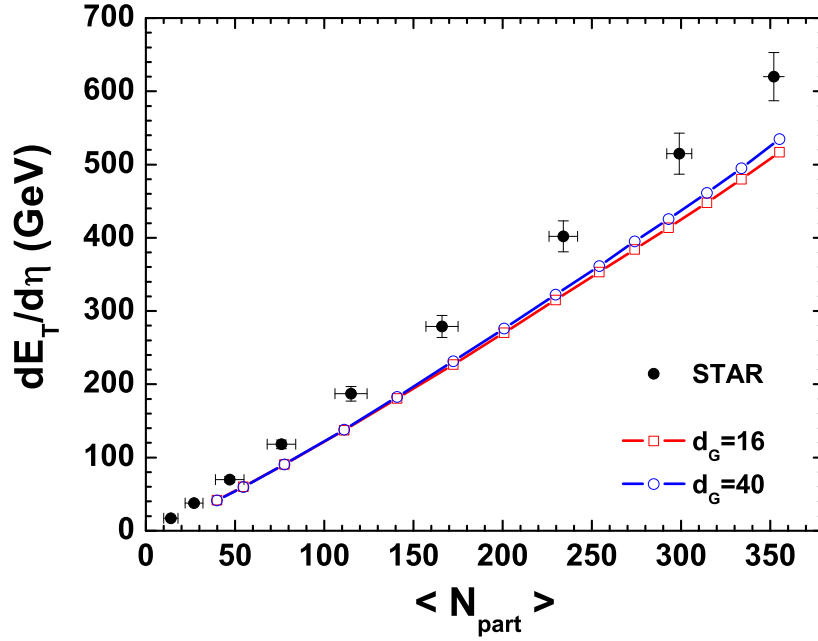


FIG. 4: (Color online) Transverse energy at midrapidity as a function of number of participating nucleons.

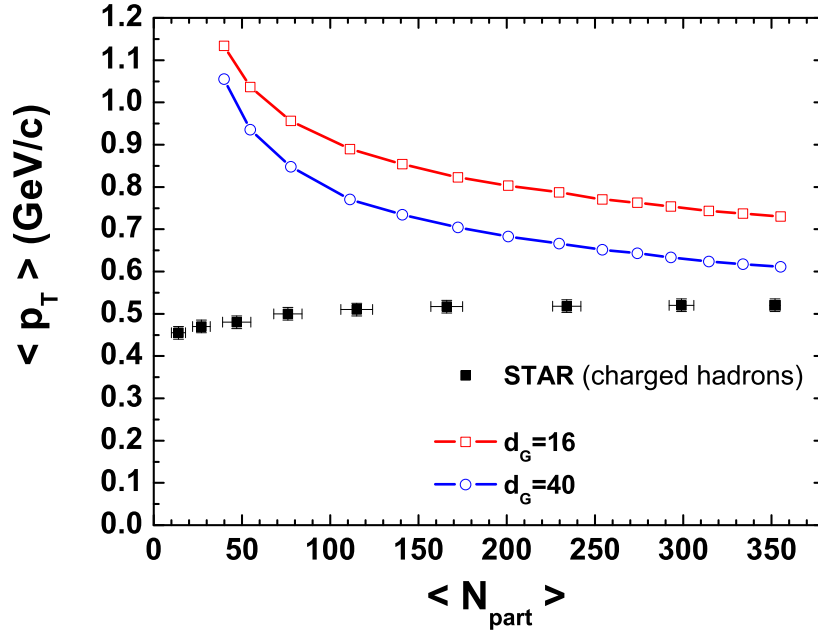


FIG. 5: (Color online) Mean transverse momentum at midrapidity as a function of number of participating nucleons, compared with the STAR data [31].

transverse energy during the expansion, which is the consequence of the same viscous effect regardless of the details of microscopical processes.

On the contrary, the mean parton transverse momentum shown in Fig. 5 does depend on the details of microscopical processes. The larger the number of parton degrees of freedom, the smaller is the final mean transverse momentum. Suppose the system is in full thermal equilibrium, we obtain the energy density  $e \sim d_G T^4$  and the particle density  $n \sim d_G T^3 \sim d_G^{1/4} e^{3/4}$ . Similar as the decrease of the transverse energy the local energy density is not sensitive to  $d_G$ . Thus,  $n \sim d_G^{1/4}$  and the particle number with  $d_G = 40$  is a factor of 1.26 more than that with  $d_G = 16$ . Therefore, to the maximum (in case of thermal equilibrium) the mean transverse momentum will be reduced by a factor of 1.26, when  $d_G$  is enlarged from 16 to 40. From Fig. 5 we realize an average reduction by a factor of 1.2, which is less than the maximum reduction. This indicates that full thermalization is not immediately achieved and particularly the net particle production (chemical equilibration) in the calculations with  $d_G = 40$  is less complete at the freeze-out than for the pure gluon system ( $d_G = 16$ ). The reason is that for the same initial condition the system with  $d_G = 40$  is initially farther apart from full chemical equilibrium than the system with  $d_G = 16$  (see Fig. 10). Because

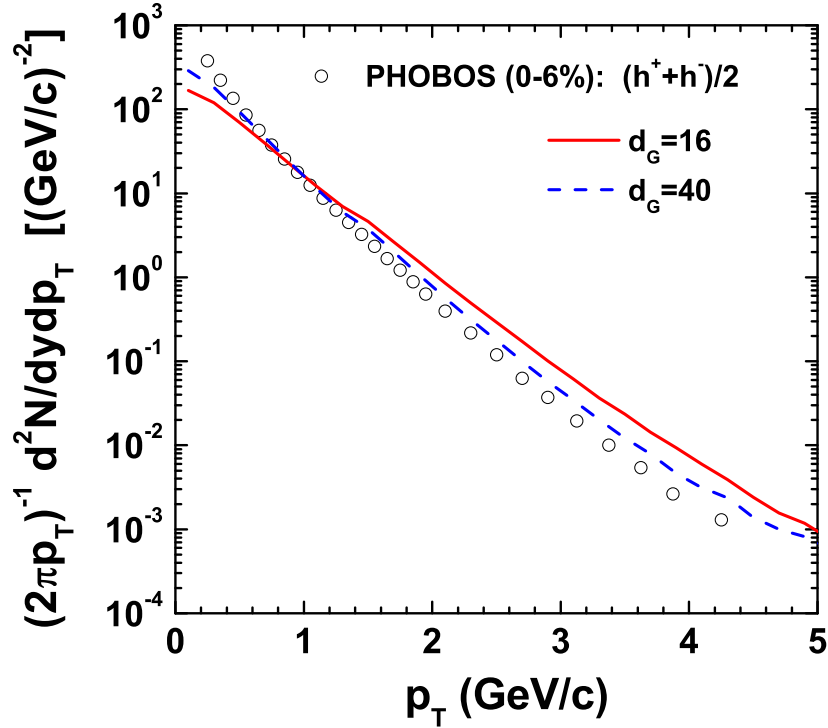


FIG. 6: (Color online) Momentum spectrum for central collisions.

the production rates  $R_{gg \rightarrow ggg}$  are almost the same in both cases, the chemical equilibration of the system with  $d_G = 40$  proceeds always behind the process in the system with  $d_G = 16$ .

The production of more particles from the same energy content leads to a smaller temperature at the (chemical) freeze-out. This clearly relates the softening of the transverse spectrum  $dN/(p_T dp_T dy)$  shown in Fig. 6 as an example for most central collisions. Both results of the mean transverse momenta and the transverse momentum spectrum come closer to the experimental data [31, 32], if the effective quark degrees of freedom are included into the parton cascade calculations.

On the one hand, the  $p_T$  averaged elliptic flow  $v_2$  is almost unchanged, when enlarging  $d_G$  from 16 to 40. On the other hand, the slope of the transverse momentum spectrum increases due to the production of more particles with larger  $d_G$ . Thus, there must be a simultaneous change in the differential elliptic flow  $v_2(p_T)$ , because  $v_2 = \int dp_T v_2(p_T) dN/N/dp_T$ . The change of  $v_2(p_T)$  is shown in Fig. 7 for the most central 50% collisions and in Fig. 8 for the mid-central class. The dotted curves are just the dashed curves times an effective factor, which enhances the  $p_T$  averaged  $v_2$  values of the calculations with  $d_G = 40$  to be equal with

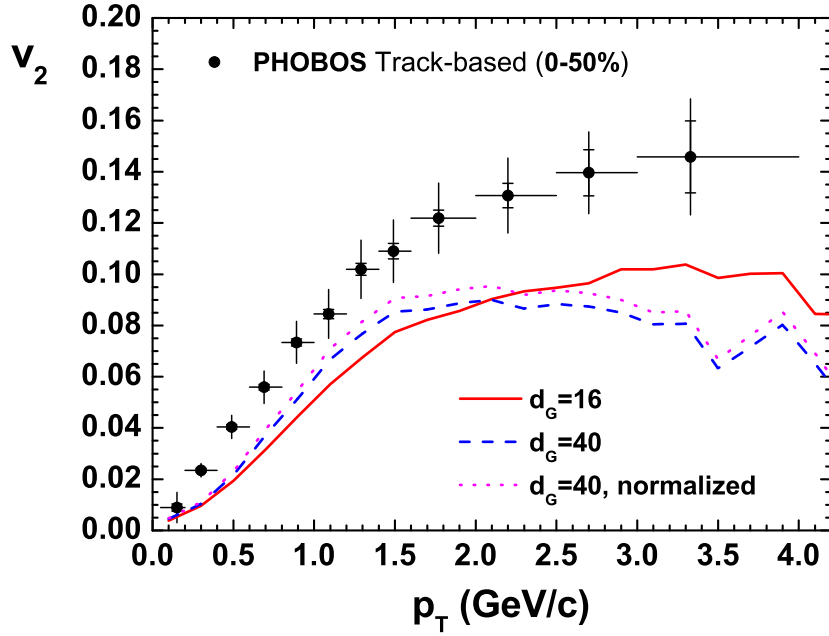


FIG. 7: (Color online) Momentum dependence of the elliptic flow  $v_2(p_T)$  for the most central 50% collisions.

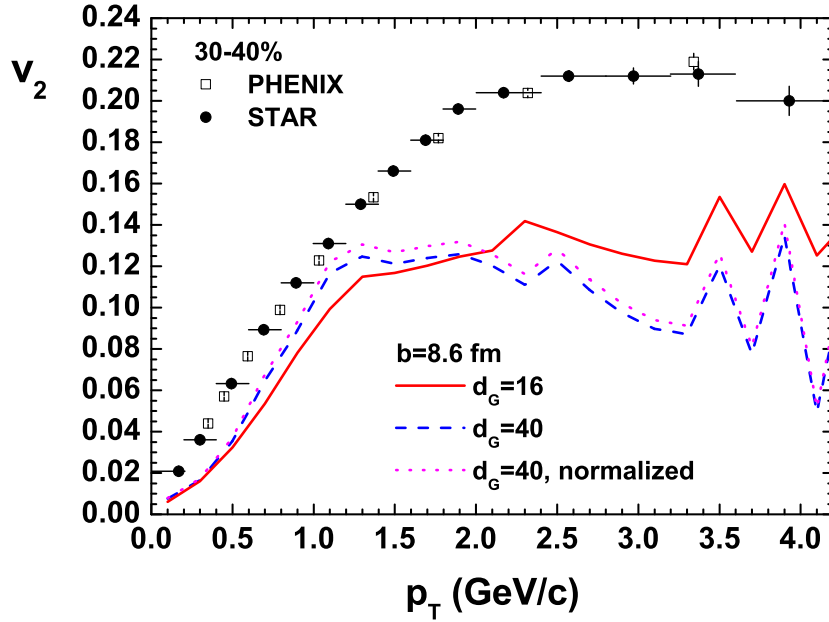


FIG. 8: (Color online) Momentum dependence of the elliptic flow  $v_2(p_T)$  for the centrality bin 30 – 40%.

those calculated using  $d_G = 16$ . The comparison between the dotted and the solid curve is then equivalent to that of the  $v_2(p_T)/v_2$  scaling. Unlike the  $p_T$  averaged  $v_2$ ,  $v_2(p_T)$  depends on the number of parton degrees of freedom: on average,  $v_2(p_T)$  moves up 20% or shifts 20% to the left toward small momentum and becomes closer to the experimental data [29, 30, 33] when quarks are added. This is the major finding of this work.

$v_2(p_T)$  values at large  $p_T$  decreases by 20% and is a factor of two smaller than the experimental data. Although this has a negligible effect on the  $p_T$  averaged  $v_2$ , because the parton number there is tiny, as seen in Fig. 6, it is important to understand hadronization. From our results we see a bend at  $p_T \approx 1.2$  GeV. For higher  $p_T$   $v_2(p_T)$  saturates. If parton recombination models [34] govern the hadronization of partons with high  $p_T$ ,  $v_2(p_T)$  of mesons will be twice of partons. This gives a reasonable explanation of the factor of two difference between the experimental data and the parton cascade  $v_2$  results at high  $p_T$ . On the other hand, viscous hydrodynamic calculations [6] showed that  $v_2$  at high  $p_T$  is very sensitive to the value of shear viscosity. Also, the difference of the viscous correction to the equilibrium phase space distribution between mesons and baryons at freeze-out can explain constituent quark scaling without quark recombinations [35]. Hadronization is still an open issue.

As a final result the shear viscosity  $\eta$  from the parton cascade simulations is extracted by using the formula, which has been derived in [36] and applied in [9]:

$$\eta \cong \frac{1}{5} n \frac{\langle E(\frac{1}{3} - v_z^2) \rangle}{\frac{1}{3} - \langle v_z^2 \rangle} \frac{1}{\sum_i R_i^{\text{tr}} + 1.5R_{gg \rightarrow ggg} - R_{ggg \rightarrow gg}}, \quad (17)$$

where  $i = gg \rightarrow gg, gg \rightarrow ggg, ggg \rightarrow gg$  and  $v_z = p_z/E$ . The transport collision rate  $R_i^{\text{tr}}$  is obtained via Eq. (16). The entropy density  $s$  is calculated by assuming the kinetic equilibrium, which gives

$$s = 4n - n \ln \lambda, \quad (18)$$

where  $\lambda = n/n_{\text{eq}}$  with  $n_{\text{eq}} = d_G T^3/\pi^2$  and  $T = e/(3n)$  defines the gluon fugacity. The true entropy density is expected to be slightly smaller, because overall kinetic equilibration cannot be complete in an expanding viscous system.

Figure 9 shows the  $\eta/s$  ratio in the center of a Au+Au collision at the impact parameter  $b = 8.6$  fm. Results from two calculations with  $d_G = 16$  (solid curve) and  $d_G = 40$  (dashed curve) are compared. At early times the  $\eta/s$  ratio from the calculation with  $d_G = 40$  is smaller than that with  $d_G = 16$ . Because the particle density  $n$  in  $\eta$  and  $s$  cancels, and quantities  $R_i^{\text{tr}}$  as shown in Fig. 2 and  $\langle E(1/3 - v_z^2) \rangle / (1/3 - \langle v_z^2 \rangle)$  are not sensitive to the

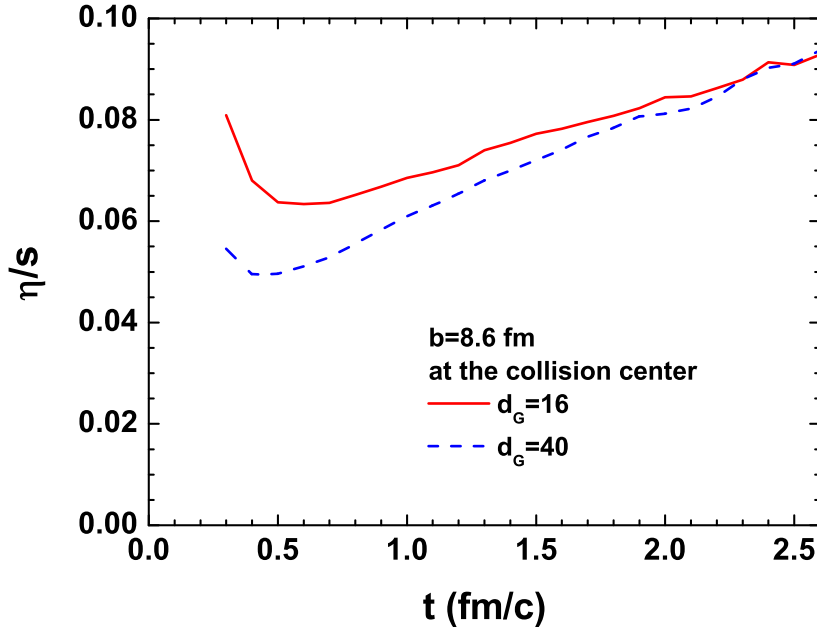


FIG. 9: (Color online) Time evolution of the ratio of the shear viscosity to the entropy density.

number of parton degrees of freedom, therefore, the difference in  $\eta/s$  comes mainly from the different chemical equilibration in two calculations, i.e., the difference in fugacity  $\lambda$ , which appears in Eq. (17) as  $1.5R_{gg \rightarrow ggg} - R_{ggg \rightarrow gg} \approx 1.5(1 - \lambda)R_{gg \rightarrow ggg}$  and in Eq. (18) as  $\ln \lambda$ .

In Fig. 10 we see that the parton fugacity  $\lambda(t)$  of the system with  $d_G = 40$  is smaller than that with  $d_G = 16$  due to the increase of parton degrees of freedom after the initial production. Smaller  $\lambda$  decreases  $\eta$  and increases  $s$ , and, thus, decreases the  $\eta/s$  ratio, especially at early times when the system is far from the chemical equilibrium. We note that the total entropy density of the quark and gluon system can only be calculated via Eq. (18), if the  $\lambda$  values of quarks and gluons are the same. In the reality, gluons dominate the early stage of the plasma and the gluon fugacity should be larger than the quark's. Therefore, the true entropy density is smaller than that obtained via Eq. (18). The true  $\eta/s$  ratio of a quark gluon plasma should be larger than that presented as the dashed curve and thus may become closer to the values for a pure gluon plasma. Moreover, the contribution of the chemical equilibration to  $\eta$ , the term  $1.5R_{gg \rightarrow ggg} - R_{ggg \rightarrow gg}$  in Eq. (17), does not appear explicitly in the expression derived in Ref. [37] by using the second order Grad's expansion. This may slightly increase  $\eta$  compared to the Navier-Stokes value via Eq. (17), if the system is out of chemical equilibrium.

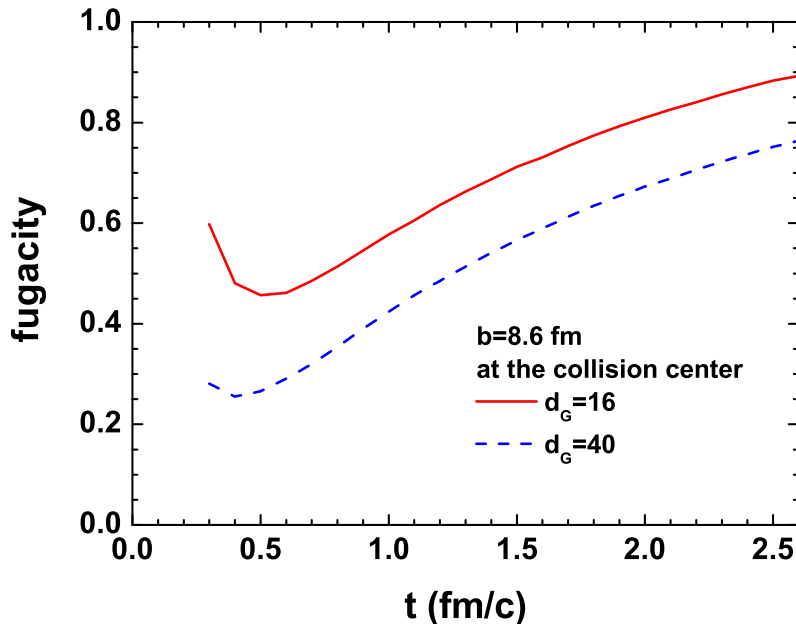


FIG. 10: (Color online) Time evolution of fugacity.

#### IV. SUMMARY

Employing the on shell parton cascade BAMPS we have studied the effect of an increasing number of parton degrees of freedom on the elliptic flow parameter  $v_2$  generated in Au+Au collisions at the RHIC energy  $\sqrt{s_{NN}} = 200$  GeV. The initial condition for BAMPS is assumed to be an ensemble of gluon minijets. The additional effective quark degrees of freedom during the further evolution are created by increasing the degeneracy factor  $d_G$  from 16 for a pure gluon system to 40 for a quark gluon system. This prescription indicates the assumption that quarks and gluons are identical particles. With this assumption for the BAMPS calculations we have found that the  $p_T$  averaged  $v_2$  values and the total transverse energy at midrapidity are almost unchanged with or without quarks, which is a consequence of the almost same transport collision rates during the entire expansion. Second, incorporating quarks the parton multiplicities at freeze-out increase, which leads to a decrease of the mean parton transverse momenta  $\langle p_T \rangle$  and a softening of the transverse spectra. Simultaneously, the differential elliptic flow  $v_2(p_T)$  shifts toward lower momentum. Adding quarks with two flavors brings a 20% effect on  $\langle p_T \rangle$  and  $v_2(p_T)$ , which is smaller than the maximum value of 26% due to the incomplete chemical equilibration in the present studies. The incomplete chemical equilibration is also the reason for the slightly smaller  $\eta/s$  value in the quark gluon



plasma compared with the result for a pure gluon plasma.

The present prescription for the inclusion of quarks gives an estimate of interactions with quarks. Bremsstrahlung involving quarks should and will be explicitly implemented in BAMPS in the future [25], because this process is essential for quantifying the thermalization and the elliptic flow of quarks. Moreover, details on the elliptic flow of both quarks and gluons at the phase transition will provide a more quantitative basis for understanding the possible effect on the elliptic flow due to the hadronization of the deconfined matter.

### Acknowledgements

The BAMPS simulations were performed at the Center for Scientific Computing of Goethe University. This work was financially supported by the Helmholtz International Center for FAIR within the framework of the LOEWE program (Landes-Offensive zur Entwicklung Wissenschaftlich-ökonomischer Exzellenz) launched by the State of Hesse.

- 
- [1] S. A. Voloshin, A. M. Poskanzer and R. Snellings, arXiv:0809.2949 [nucl-ex].
  - [2] P. Huovinen *et al.*, Phys. Lett. B **503**, 58 (2001).
  - [3] T. Schäfer and D. Teaney, Rept. Prog. Phys. **72**, 126001 (2009).
  - [4] P. Romatschke and U. Romatschke, Phys. Rev. Lett. **99**, 172301 (2007).
  - [5] H. Song and U. W. Heinz, Phys. Rev. C **77**, 064901 (2008).
  - [6] M. Luzum and P. Romatschke, Phys. Rev. C **78**, 034915 (2008) [Erratum-ibid. C **79**, 039903 (2009)].
  - [7] U. W. Heinz, arXiv:0901.4355 [nucl-th].
  - [8] D. A. Teaney, arXiv:0905.2433 [nucl-th].
  - [9] Z. Xu, C. Greiner and H. Stöcker, Phys. Rev. Lett. **101**, 082302 (2008).
  - [10] G. Ferini, M. Colonna, M. Di Toro and V. Greco, Phys. Lett. B **670**, 325 (2009).
  - [11] Z. Xu and C. Greiner, Phys. Rev. C **79**, 014904 (2009).
  - [12] H. Song and U. W. Heinz, J. Phys. G **36**, 064033 (2009).
  - [13] T. S. Biro *et al.*, Phys. Rev. C **48**, 1275 (1993).
  - [14] D. M. Elliott and D. H. Rischke, Nucl. Phys. A **671**, 583 (2000).

- [15] Z. Xu and C. Greiner, Phys. Rev. C **71**, 064901 (2005).
- [16] Z. Xu and C. Greiner, Phys. Rev. C **76**, 024911 (2007).
- [17] K. Geiger and B. Müller, Nucl. Phys. B **369**, 600 (1992); S. A. Bass, B. Müller and D. K. Srivastava, Phys. Lett. B **551**, 277 (2003).
- [18] B. Zhang, Comput. Phys. Commun. **109**, 193 (1998); Eur. Phys. J. C **62**, 25 (2009); B. Zhang, C. M. Ko, B. A. Li and Z. w. Lin, Phys. Rev. C **61**, 067901 (2000); Z. W. Lin, C. M. Ko, B. A. Li, B. Zhang and S. Pal, Phys. Rev. C **72**, 064901 (2005).
- [19] D. Molnar and M. Gyulassy, Phys. Rev. C **62**, 054907 (2000); Nucl. Phys. A **697**, 495 (2002) [Erratum-ibid. A **703**, 893 (2002)].
- [20] D. M. Zhou, X. M. Li, B. G. Dong and B. H. Sa, Phys. Lett. B **638**, 461 (2006).
- [21] C. Gombeaud and J. Y. Ollitrault, Phys. Rev. C **77**, 054904 (2008).
- [22] J. F. Gunion and G. Bertsch, Phys. Rev. D **25**, 746 (1982).
- [23] S. M. H. Wong, Nucl. Phys. A **607**, 442 (1996).
- [24] O. Fochler, Z. Xu and C. Greiner, Phys. Rev. Lett. **102**, 202301 (2009).
- [25] O. Fochler, Z. Xu, and C. Greiner, in progress.
- [26] Because Bose enhancement and Pauli blocking are not implemented in BAMPs, gluons and quarks are assumed to be Boltzmann particles, i.e.,  $f_g = f_q = \exp(-E/T)$  in equilibrium.
- [27] R. S. Bhalerao, J. P. Blaizot, N. Borghini and J. Y. Ollitrault, Phys. Lett. B **627**, 49 (2005).
- [28] The factor of  $1/3!$  in Eq. (5) of Ref. [11] is a typo and should be canceled.
- [29] J. Adams *et al.* [STAR Collaboration], Phys. Rev. C **72**, 014904 (2005).
- [30] B. B. Back *et al.* [PHOBOS Collaboration], Phys. Rev. C **72**, 051901 (2005).
- [31] J. Adams *et al.* [STAR Collaboration], Phys. Rev. C **70**, 054907 (2004).
- [32] B. B. Back *et al.* [PHOBOS Collaboration], Phys. Lett. B **578**, 297 (2004).
- [33] A. Adare *et al.* [PHENIX Collaboration], Phys. Rev. Lett. **98**, 162301 (2007).
- [34] Z. w. Lin and C. M. Ko, Phys. Rev. Lett. **89**, 202302 (2002); V. Greco, C. M. Ko and P. Levai, *ibid.* **90**, 202302 (2003); R. J. Fries, B. Müller, C. Nonaka and S. A. Bass, *ibid.* **90**, 202303 (2003); D. Molnar and S. A. Voloshin, *ibid.* **91**, 092301 (2003); R. C. Hwa and C. B. Yang, Phys. Rev. C **67**, 064902 (2003).
- [35] K. Dusling, G. D. Moore and D. Teaney, arXiv:0909.0754 [nucl-th].
- [36] Z. Xu and C. Greiner, Phys. Rev. Lett. **100**, 172301 (2008).
- [37] A. El, A. Muronga, Z. Xu and C. Greiner, Phys. Rev. C **79**, 044914 (2009).